Direct Laser Cooling of Rydberg Atoms with an Isolated-Core Transition

A. Bouillon, E. Marin-Bujedo, and M. Génévriez*
Institute of Condensed Matter and Nanosciences, Université catholique de Louvain, BE-1348 Louvain-la-Neuve, Belgium

(Received 7 February 2024; accepted 1 April 2024; published 8 May 2024)

We propose a scheme to directly laser cool Rydberg atoms by laser cooling the residual ion core within the Rydberg-electron orbit. The scheme is detailed for alkaline-earth-metal Rydberg atoms, whose ions can be easily laser cooled. We demonstrate that a closed optical cooling cycle can be found despite the perturbations caused by the Rydberg electron and that this cycle can be driven over more than 100 μs to achieve laser cooling. The cooling dynamics with and without the presence of magnetic fields are discussed in detail.

DOI: 10.1103/PhysRevLett.132.193402

Since atoms and ions were first laser cooled, opening a fascinating window into ultracold matter, sustained effort has been made to laser cool increasingly complex systems. Recent years witnessed the laser cooling of diatomic [1,2] and small polyatomic [3,4] molecules, motivated by their interest in quantum information [5] and simulation [6] or in testing the standard model [7]. Rydberg atoms are another important class of complex systems, whose large density of states and extreme sensitivity to their environment [8] are key features of many applications in quantum simulation [9–11], information [12], and optics [13]. Rydberg atoms are routinely prepared at ultracold temperatures by photoexcitation of ground state atoms in optical traps [14–17] and trapped with electric fields [18], magnetic fields [19], or optical fields [20,21]. Divalent Rydberg atoms have also been trapped in tightly focused optical tweezers [22,23]. However, Rydberg atoms have never been directly laser cooled. Doing so would open new ways to cool or manipulate ensembles of strongly interacting Rydberg atoms at low temperatures and pave the way to, e.g., combining laser cooling with tunable long-range interactions [24], exploring the thermodynamics of strongly interacting Rydberg gases [25,26], or dissipating the heat generated when Rydberg atoms are used to sympathetically cool polar molecules [27,28].

In general, the dense energy-level structure associated with the Rydberg electron is not suitable for Doppler cooling, because no closed cooling cycle is available. The only exception is between adjacent circular Rydberg states ($l = n - 1$, $|m_l| = l$), but even in this case the low photon energy associated with the transition and the long fluorescence lifetime would make cooling prohibitively slow. To overcome this difficulty, two schemes have been proposed that use atoms prepared in a coherent superposition of low-lying electronic states, which are used for laser cooling, and a Rydberg state [29,30]. In the only existing experimental work, Sr atoms with a small Rydberg character (1%) admixed to low-lying excited states were, for example, laser cooled to ∼1 μK [30]. The laser cooling of Rydberg atoms themselves, without laser dressing, is yet to be achieved.

In this Letter, we propose and theoretically analyze a scheme for directly laser cooling Rydberg atoms. It is based on the premises that, in an atom or a molecule excited to a high Rydberg state, the residual ion core is essentially *isolated* from the Rydberg electron and can be excited and optically manipulated as if it were an isolated ion [31–34]. It is then conceivable, at least in principle, to laser cool the ion core within the Rydberg-electron orbit, thereby cooling the Rydberg atom itself [see Fig. 1(a)]. We demonstrate below that, for Rydberg states of alkaline-earth atoms with high angular momentum, a strong resonant-radiation-pressure force can be applied over a timescale longer than the typical > 100 μs radiative lifetime of the Rydberg electron. Furthermore, this force is applied without significantly perturbing the Rydberg electron, an interesting feature for many applications of Rydberg atoms [9,35].

Alkaline-earth atoms are ideal systems for Rydberg-atom laser cooling, because the electronic structure of their ion core is, as for isolated ions [36], simple and well suited for Doppler cooling. We consider below the case of ^{40}Ca for illustration; however, the proposed scheme can be extended to other isotopes, other alkaline-earth species, and, in principle, any other element of the periodic table whose ion can be laser cooled. The Doppler laser cooling of $^{40}Ca^+$ involves the $4s_{1/2} - 4p_{1/2}$ transition ($A = 1.4 \times 10^8$ s^{-1}) and the $3d_{3/2} - 4p_{1/2}$ repumping transition to close the cooling cycle [Fig. 1(c)]. Our scheme for Rydberg atoms uses the same ion-core states. However, the residual Coulomb repulsion between the Rydberg electron, labeled by its principal-, orbital-angular-momentum-, and magnetic quantum numbers (n, l, m_l), and the electrons of the ion core makes the cooling dynamics more complex.

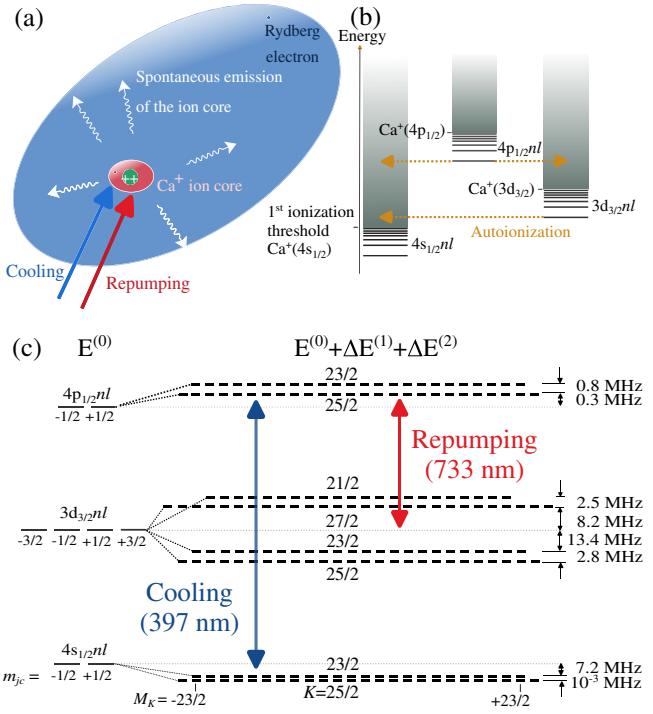

FIG. 1. (a) Schematic representation of Rydberg-atom laser cooling with an isolated-core transition. (b) Schematic view of the energy-level structure of $4s_{1/2}nl$, $4p_{1/2}nl$, and $3d_{3/2}nl$ Rydberg series. (c) Energy-level structure of the relevant ^{40}Ca Rydberg states ($n = 55$, $l = 12$), without (E^0) and with ($E^0 + \Delta E^{(1)} + \Delta E^{(2)}$) residual electron interaction. Energy splittings are in units of $h \cdot$ MHz.

First, the doubly excited states we consider here ($4p_{1/2}nl$ and $3d_{3/2}nl$) are above the first ionization threshold [Fig. 1(b)]. Because of the electronic repulsion, the atom may rapidly autoionize. Autoionization rates scale as n^{-3}, which means that autoionization could be suppressed by increasing n. This approach is, however, impractical, because, for l values close to unity, n values of the order of 1000 would be required to reach lifetimes long enough to carry out a sufficient number of cooling cycles ($\sim 10^4$) [37]. Rydberg states with such principal quantum numbers are challenging to produce experimentally and exceedingly sensitive to external perturbations [38]. Alternatively, autoionization can be suppressed by increasing l. We recently showed that the rates decay exponentially with l and that, for the typical values of $n \sim 50$ used in cold Rydberg-atom experiments, the autoionization lifetime is comparable to the Rydberg-electron radiative lifetime already for $l \gtrsim 10$ [39]. Experimentally, states with $l \sim 10$ can be prepared using Stark switching [40], whereas circular states are prepared with microwave fields or crossed electric and magnetic fields [41,42]. We consider below Ca Rydberg states with $l = 12$, the value at which the autoionization rates of all relevant states become smaller than those of the radiative decay of the Rydberg electron [39]. States with lower n and l values, which are more amenable to Stark switching, can also be used as discussed below.

The second consequence of the residual electronic correlation between the Rydberg- and ion-core electrons is the increase of the number of energy levels relevant for cooling compared to the isolated ion and the shift of their energies [Fig. 1(c)]. We detail their calculations below.

In a high-l state, the large centrifugal barrier $l(l+1)/2r^2$ that the Rydberg electron experiences prevents its penetration in the ion-core region. The Rydberg electron experiences an almost purely Coulombic potential, and its wave function is well described by a hydrogenic orbital. Because the distance between the core- and Rydberg electrons is always large, the Coulomb repulsion between them is weak and well treated within first- and second-order perturbation theory [39,43,44]. Moreover, the spin-orbit interaction of the Rydberg electron, scaling as n^{-3} [8], is negligible compared to, e.g., the natural linewidths of the cooling and repumping transitions. Rydberg states are well described within the jK coupling scheme [45], in which the total electronic angular momentum of the ion core ($\boldsymbol{j}_c$) couples to the orbital angular momentum of the Rydberg electron ($\boldsymbol{l}$) to give $\boldsymbol{K}$.

A zeroth-order electronic wave function, neglecting residual electron correlations between the Rydberg electron and the ion core, is given by

$$|n_c l_c j_c nl K M_K s m_s\rangle = \sum_{m_{j_c}, m_l} \langle j_c m_{j_c} l m_l | K M_K\rangle |n_c l_c j_c m_{j_c}\rangle |nlm_l\rangle |sm_s\rangle, \quad (1)$$

where $|n_c l_c j_c m_{j_c}\rangle$ describes the electronic wave function of the ion core and $|nlm_l\rangle$ is the Rydberg-electron orbital. We can already note that, because of angular-momentum coupling, the two degenerate magnetic sublevels that exist for $Ca^+(4s_{1/2})$ have now turned into two sets of 24 and 26 degenerate M_K sublevels associated with the $K = 23/2$ and $25/2$ levels, respectively [Fig. 1(c)].

The energy of the Rydberg states, neglecting residual electron correlations, is given by the Rydberg formula

$$E^{(0)} = E^{\mathrm{Ca}^+}_{n_c l_c j_c} - \frac{\mathrm{Ry}}{n^2}, \quad (2)$$

where Ry is the Rydberg constant for ^{40}Ca. The first-order correction $\Delta E^{(1)}$ to this energy corresponds to the interaction between the permanent quadrupole moment of the ion core $\Theta(n_c, l_c, j_c)$ and the electric field generated by the outer electron [43]:

$$\Delta E^{(1)} = (-1)^{K+j_c} \langle nl|r^{-3}|nl\rangle (2l+1)\Theta(n_c, l_c, j_c) \times \begin{pmatrix} l & 2 & l \\ 0 & 0 & 0 \end{pmatrix} \begin{Bmatrix} K & l & j_c \\ 2 & j_c & l \end{Bmatrix} \Big/ \begin{pmatrix} j_c & 2 & j_c \\ j_c & 0 & -j_c \end{pmatrix}. \quad (3)$$

Because of symmetry, it is nonvanishing for the $3d_{3/2}$ ion-core state only, which explains the greater energy shifts of the associated Rydberg states compared to the $4s_{1/2}$ and $4p_{1/2}$ ion-core states. The second-order energy correction $\Delta E^{(2)}$ corresponds to the polarization of the ion core by the outer electron. Its expression is more complex and given in [44].

We calculated the first- and second-order energy corrections using known multipole moments, matrix elements, and polarizabilities of Ca^+ [46–48]. The resulting energy-level structure of the Ca Rydberg levels involved in the cooling cycle is shown in Fig. 1(c) for $n = 55$ and $l = 12$. Each ion-core state is shifted and split into several K levels with different energies. Whereas the energy splittings between the different K states of the $4s_{1/2}$ and $4p_{1/2}$ core levels are small (< 1 MHz) and, in fact, smaller than the natural linewidth of the $4s_{1/2} - 4p_{1/2}$ cooling transition and the $3d_{3/2} - 4p_{1/2}$ repumping transition (24 MHz), the splittings for the $3d_{3/2}$ core level are larger (up to 26.9 MHz for the outermost K states).

To check the validity and accuracy of the perturbative treatment presented above, we compared the energy shifts $\Delta E^{(1)} + \Delta E^{(2)}$ against those we obtained from nonperturbative *ab initio* calculations using the method of configuration interaction with exterior complex scaling (CI-ECS) [49,50]. Briefly, CI-ECS treats the motion of the two valence electrons of Ca explicitly and without approximation, whereas the effect of the closed shell Ca^{2+} core is accounted for with a model potential [50]. The large two-electron Hamiltonian is calculated and diagonalized in a basis of two-electron functions built from numerical basis functions [51] and using exterior-complex scaling to describe continuum processes such as autoionization. Details on the CI-ECS calculations can be found in Ref. [39]. The differences between the perturbative and CI-ECS energies for the $4s_{1/2}nl$, $4p_{1/2}nl$, and $3d_{3/2}nl$ Rydberg states are very small (< 1 MHz), which validates the perturbative approach. The CI-ECS results also confirm that channel interactions, which are not accounted for in the single-configuration perturbative model described above, are negligible for the states under consideration. Overall, CI-ECS calculations are much more computationally heavy than perturbative ones. This precludes their use to simulate the time-dependent photoexcitation and cooling dynamics, to which we now turn.

When light is close to resonance with a transition in the isolated ion, Rydberg atoms are known to undergo isolated-core excitation (ICE) [31]. The ion core, which is to a good approximation isolated from the Rydberg electron, is resonantly excited as if it were an isolated ion, while the Rydberg electron, whose interaction with the radiation is negligible in comparison, is a spectator of the core excitation (see Refs. [40,52] for recent examples). The electric dipole moment of the $4s_{1/2}nl_K - 4p_{1/2}n'l'_{K'}$ transition can be written as [53]

$$\begin{aligned}&\langle 4p_{1/2}n'l'K'M'_K|\hat{\boldsymbol{D}}|4s_{1/2}nlKM_K\rangle \\ &\simeq (-1)^{2K-M'_K-l-j'_c}[K,K']^{1/2}\bar{\mu}_c\langle n'l'|nl\rangle \\ &\quad\times\begin{pmatrix} K & 1 & K' \\ M_K & q & -M'_K\end{pmatrix}\begin{Bmatrix} K' & 1 & K \\ 1/2 & l & 1/2\end{Bmatrix},\end{aligned} \tag{4}$$

where the right-hand side is obtained using Eq. (1) and assuming that the transition dipole moment for the Rydberg electron $\langle n'l'|\boldsymbol{\epsilon}\cdot\boldsymbol{r}|nl\rangle$ is vanishingly small. We used the standard notation $[K] = 2K + 1$. The Wigner $3j$ and $6j$ symbols result from angular momentum coupling, and $\bar{\mu}_c$ is the reduced dipole moment of the $Ca^+(4s_{1/2} - 4p_{1/2})$ transition. $\langle n'l'|nl\rangle$ is the overlap integral between the initial and final Rydberg-electron wave functions. Because the Rydberg electron is quasihydrogenic, the overlap integral is 1 if $n = n'$ and $l' = l$ and 0 otherwise. Importantly, this shows that the state of the Rydberg electron is left unchanged upon ICE. Equation (4) also yields the ICE selection rules $\Delta K = 0, \pm 1$ and $\Delta M_K = q$, where $q = 0, \pm 1$ for π and $\sigma^{\pm}$ polarizations, respectively. A similar expression is obtained for the repumping transition.

Population dynamics when driving the cooling and repumping ICE transitions were calculated by numerically solving the Lindblad master equation [54] for the 200-level system shown in Fig. 1. Rabi frequencies and fluorescence rates obtained from Eq. (4) were included together with the energies calculated with the perturbative approach and the autoionization rates reported in Ref. [39]. The latter rates ($< 10^3$ s^{-1}) do not produce observable population losses over the timescale of the calculations (100 μs), whose duration was chosen to correspond to the blackbody-radiation lifetime [8] of an $n = 55$, $l = 12$ Rydberg electron.

Laser parameters for the calculation were chosen based on a detailed study performed to optimize the cooling of trapped alkaline-earth ions [55]. The cooling-laser intensity is equal to the saturation intensity of the $Ca^+(4s_{1/2} - 4p_{1/2})$ transition ($I_s = 4.66 \times 10^{-4}$ W mm^{-2}) and the detuning relative to that transition is $\Delta\omega_c/2\pi = 7.7$ MHz, a value that compensates the energy-level shifts $\Delta E^{(2)}$ (see Fig. 1). The repumping-laser intensity is $I_r = I_s$, and its detuning relative to the $Ca^+(3d_{3/2} - 4p_{1/2})$ transition is $\Delta\omega_c/2\pi = 3.2$ MHz. We assume that the Rydberg atom is initially prepared in the $4s_{1/2}55(l = 12)_{K=23/2}$ state with $M_K = 1/2$, which corresponds to the typical states populated in Stark-switching experiments [56]. We also verified that starting from another K and M_K state, as would be the case if, for example, a circular Rydberg state were considered [57], does not change the overall dynamics nor the conclusions drawn below.

Figure 2 shows the population dynamics and photon-scattering rate Γ when both lasers have π polarizations. It is

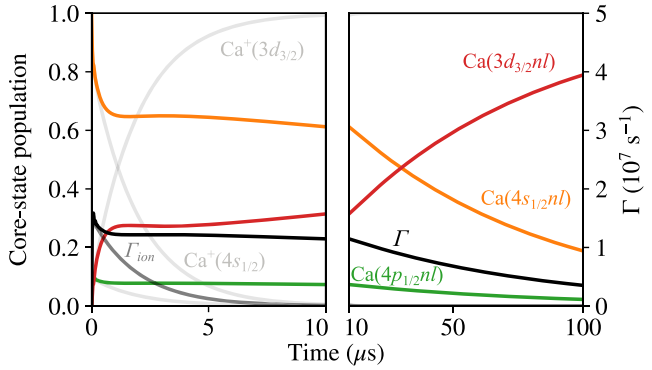

FIG. 2. Time evolution of the populations of Rydberg states ($n = 55$, $l = 12$) with $4s_{1/2}$ (orange line), $3d_{3/2}$ (red line), and $4p_{1/2}$ (green line) ion-core states, obtained by summing the populations of states with different values of K and M_K but identical values of n_c, l_c, and j_c. The photon-scattering rate Γ for the cooling transition is shown as the black line. The dynamics for the isolated ion are shown by the pale gray lines.

well known that, in the isolated ion and for π polarizations, the population is rapidly pumped into the $3d_{3/2}(|m_j| = 3/2)$ dark states and the photon-scattering rate drops to zero (light gray lines in Fig. 2) [55]. The same dynamics occur in the Rydberg atom but over a much longer timescale, with a dark-state pumping rate determined to be $\Gamma_{\rm DS} = 1.3 \times 10^4$ s^{-1}. The reason for this lower rate is that the population of the states with an excited $4p_{1/2}$ ion core is now distributed over the 50 different M_K sublevels ($K = 23/2, 25/2$), and only two of those sublevels can fluoresce to the $3d_{3/2}55(l = 12)_{27/2}$, $|M_K| = 27/2$ dark states (see Fig. 1). When the lasers have σ^+ or σ^- polarizations, the system decays much faster into a dark state.

The results in Fig. 2 reveal that light can be scattered by the ion core of a Rydberg atom at a rate of up to $\sim 10^7$ s^{-1}, a value similar to the one of the isolated ion. Such a rate translates into a resonant-radiation-pressure force of 2×10^{-20} N and a deceleration of the ^{40}Ca Rydberg atoms of 3×10^4 g. Even in the absence of a strategy to destabilize dark states, photon scattering is efficient beyond the 10-μs range, a timescale over which the atoms can be, e.g., cooled or deflected in optical molasses.

To achieve laser-cooling durations over the entire radiative lifetime of the Rydberg electron, the dark states must be destabilized by, e.g., periodically switching the laser polarization or applying a magnetic field [55,58]. We consider below the magnetic-field case, which further offers the opportunity to assess the effect of stray magnetic fields present in experiments. For a magnetic field B of moderate strength, the ion core undergoes a Zeeman effect in the weak-field limit, whereas for the Rydberg electron it is well into the Paschen-Back regime [8], because the spin-orbit interaction is very small. The Zeeman Hamiltonian is then diagonal in the $|KM_K\rangle$ basis with eigenvalues given by

$$\Delta E^{\rm Zeeman}_{K,M_K} = \mu_B B \sum_{m_{j_c},m_l} \langle j_c m_{j_c} l m_l | K M_K \rangle^2 \times [g_{j_c} m_{j_c} + m_l + g_s m_s], \quad (5)$$

where g_{j_c} and g_s are the ion-core and Rydberg-electron g factors, respectively. The energy level structure of the Zeeman-split levels is shown in Fig. 3(a) for a magnetic field $B = 20$ μT. The splitting between two adjacent M_K levels is ∼0.3 MHz, a value sufficient to destabilize the dark states at a rate larger than $\Gamma_{\rm DS}$.

Population dynamics calculated for a π-polarized cooling laser and a repumping laser that is elliptically polarized (90% of the intensity in σ^+ and 10% in σ^-) are shown in Fig. 3(b). These polarizations were chosen to illustrate two effects. First, the magnetic field effectively removes the dark states, and a photon-scattering rate of $\sim 10^7$ s^{-1} can be maintained beyond 100 μs. A field of 20 μT is weaker than the typical Earth magnetic field, and, therefore, unless residual magnetic fields are actively compensated in an experiment, they will destabilize dark states and allow Rydberg-atom laser cooling over long timescales. Second, by choosing an appropriate polarization for the repumping laser, the atoms can be optically pumped into, predominantly, the largest M_K sublevels [see Fig. 3(b)]. Other ellipticities for the repumping-laser polarization influence slightly the degree of optical pumping and the photon-scattering rate; however, a large Γ can still be maintained beyond 100 μs as well.

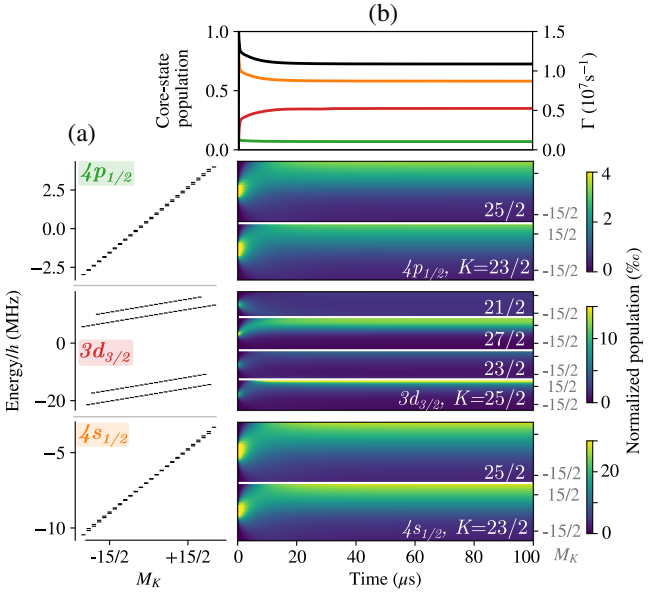

FIG. 3. (a) Energy levels of the $4s_{1/2}nl_{KM_K}$, $3d_{3/2}nl_{KM_K}$, and $4p_{1/2}nl_{KM_K}$ states in the presence of a 20 μT magnetic field ($n = 55$, $l = 12$). (b) Top graph: time evolution of the ion-core populations and photon-scattering rate (the same as Fig. 2). Lower graphs: time evolution of the population of each of the 200 sublevels involved in the cooling.

Large photon-scattering rates can also be achieved for stronger magnetic fields. For example, for $B = 6$ mT, the Zeeman shifts of the $\Delta M_K = \pm 1$ transitions (approximately ± 84 MHz) can be compensated by tuning the frequencies of the σ^+ and σ^- components of the cooling and repumping lasers accordingly, reaching $\Gamma > 5 \times 10^6\ \mathrm{s}^{-1}$. Interestingly, the tunability of the cooling-transition frequency with an external magnetic field makes it possible to address Doppler shifts and laser cool relatively warm Rydberg atoms, much as in conventional Zeeman slowers and magneto-optical traps. Velocities in the 35-m/s range ($E/k_B \sim 3$ K) could be addressed with $B = 6$ mT, which corresponds to typical velocities of atoms exiting a Zeeman slower or a buffer-gas cooling cell [59]. Such atom sources are, thus, ideal for future experimental implementations of Rydberg-atom laser cooling. Larger velocities and temperatures can also be targeted to optically deflect or manipulate Rydberg atoms, within the limitations imposed by the Stark-switching process and the radiative lifetime of the Rydberg electron.

For $n \sim 50$, we estimate that Rydberg-atom densities larger than $N_0 \sim 10^{10}\ \mathrm{cm}^{-3}$ can be reached. At such densities, the Rydberg atoms are separated by 5 μm on average. Long-range dipole-dipole interactions shift the energy levels by ∼15 MHz [8], a value comparable to the width of the cooling transition. However, the cooling transition can shift less than the levels themselves; therefore, N_0 represents a lower bound of the achievable atomic density. A better estimate of N_0 can be obtained only from accurate calculations of long-range interactions, which are currently unavailable.

We finally discuss the range of n and l values for which the method is applicable. The population in the $4p_{1/2}nl_K$ excited states is ∼0.1, and, therefore, the rate at which the Rydberg atoms autoionize under laser cooling is one order of magnitude lower than the one of pure $4p_{1/2}nl_K$ states. This argument holds because the $3d_{3/2}nl_K$ states autoionize at a rate 2 orders of magnitude smaller than $4p_{1/2}nl_K$ ones [39]. Taking the autoionization rates calculated in [39], the present Rydberg-atom laser-cooling scheme is applicable, for ^{40}Ca, to $n > 40$ for $l = 10$ and $n \geq 13$ for $l \geq 11$. In the Sr atom, the larger autoionization rates lead to the cooling scheme being applicable to $n \geq 32$ for $l = 11$ and $n \geq 13$ for $l \geq 12$. Such states (e.g., $n = 17$, $l = 12$) have been populated by Stark switching in earlier experiments [60].

In conclusion, we have presented a strategy to directly and selectively cool Rydberg atoms using isolated-core excitation. It requires high l ($l \gtrsim 10$) Rydberg states to prevent the atoms from autoionizing as they are cooled. Efficient cooling, with a photon-scattering rate of $10^7\ \mathrm{s}^{-1}$, can be maintained over more than 100 μs, i.e., over the radiative lifetime of the Rydberg electron. Because the Rydberg electron is essentially hydrogenic, the details of the ion-core structure are expected to have little influence on the cooling strategy presented above, which should, thus, be applicable to isotopes and species other than ^{40}Ca. The present work paves the way to an experimental demonstration of direct and selective Rydberg-atom laser cooling, a result of importance for quantum simulation and metrology. It provides a way to produce ultracold clouds of *only* Rydberg atoms and to control their temperature, thus permitting the exploration of the thermodynamical properties of strongly interacting Rydberg gases as a function of temperature.

This work was supported by the Fonds de la Recherche Scientifique—FNRS under MIS Grant No. F.4027.24 and IISN Grant No. 4.4504.10. E. M.-B. is supported by the Fonds de la Recherche Scientifique—FNRS. E. M.-B. and M. G. acknowledge support from the Fonds Spéciaux de Recherche (FSR) of UCLouvain.

*matthieu.genevriez@uclouvain.be

[1] E. S. Shuman, J. F. Barry, and D. DeMille, Nature (London) **467**, 820 (2010).
[2] V. Zhelyazkova, A. Cournol, T. E. Wall, A. Matsushima, J. J. Hudson, E. A. Hinds, M. R. Tarbutt, and B. E. Sauer, Phys. Rev. A **89**, 053416 (2014).
[3] I. Kozyryev, L. Baum, K. Matsuda, B. L. Augenbraun, L. Anderegg, A. P. Sedlack, and J. M. Doyle, Phys. Rev. Lett. **118**, 173201 (2017).
[4] D. Mitra, N. B. Vilas, C. Hallas, L. Anderegg, B. L. Augenbraun, L. Baum, C. Miller, S. Raval, and J. M. Doyle, Science **369**, 1366 (2020).
[5] D. DeMille, Phys. Rev. Lett. **88**, 067901 (2002).
[6] J. A. Blackmore, L. Caldwell, P. D. Gregory, E. M. Bridge, R. Sawant, J. Aldegunde, J. Mur-Petit, D. Jaksch, J. M. Hutson, B. E. Sauer, M. R. Tarbutt, and S. L. Cornish, Quantum Sci. Technol. **4**, 014010 (2018).
[7] B. L. Augenbraun, Z. D. Lasner, A. Frenett, H. Sawaoka, C. Miller, T. C. Steimle, and J. M. Doyle, New J. Phys. **22**, 022003 (2020).
[8] T. F. Gallagher, *Rydberg Atoms*, Cambridge Monographs on Atomic, Molecular and Chemical Physics (Cambridge University Press, Cambridge, England, 1994), 10.1017/CBO9780511524530.
[9] A. Browaeys and T. Lahaye, Nat. Phys. **16**, 132 (2020).
[10] S. Whitlock, A. W. Glaetzle, and P. Hannaford, J. Phys. B **50**, 074001 (2017).
[11] T. L. Nguyen, J. M. Raimond, C. Sayrin, R. Cortiñas, T. Cantat-Moltrecht, F. Assemat, I. Dotsenko, S. Gleyzes, S. Haroche, G. Roux, T. Jolicoeur, and M. Brune, Phys. Rev. X **8**, 011032 (2018).
[12] S. R. Cohen and J. D. Thompson, PRX Quantum **2**, 030322 (2021).
[13] C. S. Adams, J. D. Pritchard, and J. P. Shaffer, J. Phys. B **53**, 012002 (2019).
[14] A. Walz-Flannigan, J. R. Guest, J.-H. Choi, and G. Raithel, Phys. Rev. A **69**, 063405 (2004).
[15] R. Côté, A. Russell, E. E. Eyler, and P. L. Gould, New J. Phys. **8**, 156 (2006).
[16] T. Macrì and T. Pohl, Phys. Rev. A **89**, 011402(R) (2014).

[17] M. Endres, H. Bernien, A. Keesling, H. Levine, E. R. Anschuetz, A. Krajenbrink, C. Senko, V. Vuletic, M. Greiner, and M. D. Lukin, Science **354**, 1024 (2016).
[18] S. D. Hogan and F. Merkt, Phys. Rev. Lett. **100**, 043001 (2008).
[19] J.-H. Choi, J. R. Guest, A. P. Povilus, E. Hansis, and G. Raithel, Phys. Rev. Lett. **95**, 243001 (2005).
[20] R. Mukherjee, J. Millen, R. Nath, M. P. A. Jones, and T. Pohl, J. Phys. B **44**, 184010 (2011).
[21] R. G. Cortiñas, M. Favier, B. Ravon, P. Méhaignerie, Y. Machu, J. M. Raimond, C. Sayrin, and M. Brune, Phys. Rev. Lett. **124**, 123201 (2020).
[22] J. T. Wilson, S. Saskin, Y. Meng, S. Ma, R. Dilip, A. P. Burgers, and J. D. Thompson, Phys. Rev. Lett. **128**, 033201 (2022).
[23] C. Hölzl, A. Götzelmann, E. Pultinevicius, M. Wirth, and F. Meinert, Phys. Rev. X **14**, 021024 (2024).
[24] A. W. Glaetzle, R. Nath, B. Zhao, G. Pupillo, and P. Zoller, Phys. Rev. A **86**, 043403 (2012).
[25] O. N. Osychenko, G. E. Astrakharchik, Y. Lutsyshyn, Yu. E. Lozovik, and J. Boronat, Phys. Rev. A **84**, 063621 (2011).
[26] M. Brune and D. J. Papoular, Phys. Rev. Res. **2**, 023014 (2020).
[27] C. Zhang, S. T. Rittenhouse, T. V. Tscherbul, H. R. Sadeghpour, and N. R. Hutzler, Phys. Rev. Lett. **132**, 033001 (2024).
[28] B. Zhao, A. W. Glaetzle, G. Pupillo, and P. Zoller, Phys. Rev. Lett. **108**, 193007 (2012).
[29] J. Guo and E. Arimondo, Phys. Rev. A **53**, R1224 (1996).
[30] A. D. Bounds, N. C. Jackson, R. K. Hanley, R. Faoro, E. M. Bridge, P. Huillery, and M. P. A. Jones, Phys. Rev. Lett. **120**, 183401 (2018).
[31] W. E. Cooke, T. F. Gallagher, S. A. Edelstein, and R. M. Hill, Phys. Rev. Lett. **40**, 178 (1978).
[32] D. Wehrli, M. Génévriez, and F. Merkt, Phys. Rev. A **100**, 012515 (2019).
[33] M. Génévriez, D. Wehrli, T. Berglitsch, and F. Merkt, Phys. Rev. A **104**, 042811 (2021).
[34] A. Muni, L. Lachaud, A. Couto, M. Poirier, R. C. Teixeira, J.-M. Raimond, M. Brune, and S. Gleyzes, Nat. Phys. **18**, 502 (2022).
[35] M. Saffman, T. G. Walker, and K. Mølmer, Rev. Mod. Phys. **82**, 2313 (2010).
[36] J. Eschner, G. Morigi, F. Schmidt-Kaler, and R. Blatt, J. Opt. Soc. Am. B **20**, 1003 (2003).
[37] G. Fields, X. Zhang, F. B. Dunning, S. Yoshida, and J. Burgdörfer, Phys. Rev. A **97**, 013429 (2018).
[38] S. Ye, X. Zhang, T. C. Killian, F. B. Dunning, M. Hiller, S. Yoshida, S. Nagele, and J. Burgdörfer, Phys. Rev. A **88**, 043430 (2013).
[39] E. Marin-Bujedo and M. Génévriez, Phys. Rev. A **108**, 012816 (2023).
[40] H. Lehec, X. Hua, P. Pillet, and P. Cheinet, Phys. Rev. A **103**, 022806 (2021).
[41] A. A. Morgan, V. Zhelyazkova, and S. D. Hogan, Phys. Rev. A **98**, 043416 (2018).
[42] R. G. Hulet and D. Kleppner, Phys. Rev. Lett. **51**, 1430 (1983).
[43] L. Chen, M. Chéret, M. Poirier, F. Roussel, T. Bolzinger, and G. Spiess, J. Phys. II France **2**, 701 (1992), see equation (A5).
[44] E. S. Shuman and T. F. Gallagher, Phys. Rev. A **74**, 022502 (2006).
[45] M. Aymar, C. H. Greene, and E. Luc-Koenig, Rev. Mod. Phys. **68**, 1015 (1996).
[46] M. S. Safronova and U. I. Safronova, Phys. Rev. A **83**, 012503 (2011).
[47] S. Singh, M. Kaur, B. Arora, and B. K. Sahoo, Phys. Rev. A **98**, 013406 (2018).
[48] M. Kaur, S. Singh, B. Sahoo, and B. Arora, At. Data Nucl. Data Tables **140**, 101422 (2021).
[49] M. Génévriez, D. Wehrli, and F. Merkt, Phys. Rev. A **100**, 032517 (2019).
[50] M. Génévriez, Mol. Phys. **119**, e1861353 (2021).
[51] T. N. Rescigno and C. W. McCurdy, Phys. Rev. A **62**, 032706 (2000).
[52] S. Yoshida, J. Burgdörfer, R. Brienza, G. Fields, and F. B. Dunning, Phys. Rev. A **107**, 043112 (2023).
[53] S. A. Bhatti, C. L. Cromer, and W. E. Cooke, Phys. Rev. A **24**, 161 (1981).
[54] J. R. Johansson, P. D. Nation, and F. Nori, Comput. Phys. Commun. **183**, 1760 (2012).
[55] T. Lindvall, M. Merimaa, I. Tittonen, and A. A. Madej, Phys. Rev. A **86**, 033403 (2012).
[56] R. R. Freeman and D. Kleppner, Phys. Rev. A **14**, 1614 (1976).
[57] R. C. Teixeira, A. Larrouy, A. Muni, L. Lachaud, J.-M. Raimond, S. Gleyzes, and M. Brune, Phys. Rev. Lett. **125**, 263001 (2020).
[58] D. J. Berkeland and M. G. Boshier, Phys. Rev. A **65**, 033413 (2002).
[59] N. R. Hutzler, H.-I. Lu, and J. M. Doyle, Chem. Rev. **112**, 4803 (2012).
[60] U. Eichmann, T. F. Gallagher, and R. M. Konik, Phys. Rev. Lett. **90**, 233004 (2003).